Optical Materials 51 (2016) 35–41

Contents lists available at ScienceDirect

Optical Materials

journal homepage: www.elsevier.com/locate/optmat

Nd^{3+}-doped TeO_2–PbF_2–AlF_3 glasses for laser applications

E.A. Lalla [a,b], U.R. Rodríguez-Mendoza [a,c,*], A.D. Lozano-Gorrín [a], A. Sanz-Arranz [b], F. Rull [b], V. Lavín [a,d]

[a] Departamento de Física, Universidad de La Laguna, 38200 San Cristóbal de La Laguna, Santa Cruz de Tenerife, Spain
[b] Unidad Asociada Uva-CSIC al Centro de Astrobiología CSIC-INTA "ERICA", Parque Tecnológico de Boecillo, 47151 Boecillo, Valladolid, Spain
[c] Instituto Universitario de Materiales y Nanotecnología, Universidad de La Laguna, 38200 San Cristóbal de La Laguna, Santa Cruz de Tenerife, Spain
[d] Instituto Universitario de Estudios Avanzados en Atómica, Molecular y Fotónica, Av. Francisco Sánchez s/n, Universidad de La Laguna, 38200 San Cristóbal de La Laguna, Tenerife, Spain

ARTICLE INFO

Article history:
Received 5 October 2015
Received in revised form 5 November 2015
Accepted 6 November 2015

Keywords:
Nd^{3+} ions
Fluorotellurite glasses
Judd–Ofelt analysis
Emission and absorption cross-sections
Laser hosts

ABSTRACT

A study of the optical properties of Nd^{3+} ion in TeO_2–PbF_2–AlF_3 glasses has been carried out for different Nd^{3+} concentrations. Based on the Judd–Ofelt theory, intensity parameters and radiative properties were determined from the absorption spectra. Focusing on the suitability of this host for laser applications, the spectroscopic quality factor χ was obtained with a value of 1.07, a value of the order of other compositions proposed as laser hosts. For the most intense emission corresponding with the $^4F_{3/2} \rightarrow {}^4I_{11/2}$ transition (1.06 μm), the absorption and emission and have been calculated with values of 1.20×10^{-20} cm^2, 2.08×10^{-20} cm^2. A positive value for the gain cross-sections has been found for a population inversion factor γ of 0.4 in the spectral range from 1060 to 1110 nm. All these results suggest the potentially use of this system as a laser host.

1. Introduction

Nowadays the search of suitable materials for photonics applications has conducted to the synthesis of several trivalent rare earths (RE^{3+}) doped matrices, comprising crystals, glass–ceramics and glasses. Particularly, the glasses offer advantages in comparison with other hosts, owing to lower costs and simpler methods of preparation. For this reason, the optical characterization of glasses doped with RE^{3+} ions have been extensively investigated due to their multiple applications, including optical amplifiers, upconverters and laser applications [1–3]. Among the common requirements that must fulfill the glasses hosts highlight wide transmission ranges from ultraviolet (UV) to mid-infrared (IR), good chemical, mechanical and thermal stabilities, high non-linear refractive index, and relatively low-energy phonon, which reduce the multiphonon non-radiative probabilities and, consequently, increase the quantum yields. In this regard, glasses such as chalcogenides, borates, fluorozirconates, fluorides, silicates [4–6] and tellurites have been the subject of several extensive studies.

In our case, a combination of tellurites and fluorides has been used for the synthesis of a Nd^{3+}-doped fluorotellurite glass. The tellurite glasses containing 60–90% of TeO_2 units, as a glass former, need to be combined with modifier compounds in order to easily form a glassy state. In terms of high transmission in the VIS–NIR range and low-energy phonons matrices, fluorides seem to be good candidates [5]. Thus the multicomponent glasses combination of tellurium oxides and heavy metal fluorides has been demonstrated to be matrices with the advantages of both component systems, becoming excellent for EDFA at 1.5 μm band when it is doped with Er^{3+} ions [7]. Similar multicomponent materials based on doped tellurite glasses had shown promising applications for amorphous solar cells concentrators [8–10], taking advantage of the up- and down- conversion processes and incorporating layers above (for down-conversion and photoluminescence) or below (for up-conversion) to improve the energy efficiencies [9]. In this sense, several RE^{3+} combinations such as Er^{3+}/Yb^{3+}, $Ce^{3+}/Er^{3+}/Yb^{3+}$ and Yb^{3+}/Tb^{3+} have been tested in order to increase the quantum efficiency of conventional solar cells [9–12].

In this work the optical properties of Nd^{3+}-doped TeO_2–PbF_2–AlF_3 glasses have been investigated. In order to test the suitability for laser applications in the near infrared (NIR), special attention has been paid to the 1.06 μm emission of the Nd^{3+} ion corresponding to the $^4F_{3/2} \rightarrow {}^4I_{11/2}$ transition. Indeed, Nd^{3+} is one of the most studied RE^{3+} ions and it is also one the most efficient candidates for photonic devices [13], owing to the suitability in emitting in the NIR which makes it the best possible candidate for high-power laser applications, in which high gain, energy storage capacity and low optical losses are required. Nevertheless, for

* Corresponding author at: Departamento de Física, Universidad de La Laguna, 38200 San Cristóbal de La Laguna, Santa Cruz de Tenerife, Spain.
E-mail address: urguez@ull.edu.es (U.R. Rodríguez-Mendoza).

http://dx.doi.org/10.1016/j.optmat.2015.11.010
0925-3467/

suitable applications in ultra-fast spectroscopic investigations and non-heating laser processing it is necessary to develop high-average power, high-efficiency, compacts and low-cost femtosecond lasers. In this regard, the transitions at $^4F_{3/2} \rightarrow {}^4I_{13/2}$ (~915 nm), $^4F_{3/2} \rightarrow {}^4I_{11/2}$ (~1065 nm) and $^4F_{3/2} \rightarrow {}^4I_{9/2}$ (~1340 nm) in the NIR-range are the most suitable for the commented applications [6].

We will focus on the more intense band corresponding to the $^4F_{3/2} \rightarrow {}^4I_{11/2}$ transition. Several results have been reported on the luminescent properties of Nd^{3+} ions in a variety of glass matrices which include silicates [14], borates [6], tellurites [15] and chalocogenides [16]. Thus, the luminescent properties of the Nd^{3+} ions are considerably modified by suitably selecting the network of the forming and the modifying cations. In this work, the $85TeO_2$–$10PbF_2$–$(5-x)AlF_3$–$xNdF_3$ ($x = 0.01$, 0.5 and 2.5) glasses have been characterized by means of X-ray diffraction (XRD), differential scanning calorimetry (DSC), Raman and optical spectroscopy. An estimation of the spontaneous radiative emission probabilities for each transition of the Nd^{3+} ion was calculated from the optical absorption spectrum through the Judd–Ofelt (J–O) theory [17,18]. The emission spectra as well as the decay curves have been analyzed as a function of the Nd^{3+} concentration, with special attention to the NIR $^4F_{3/2} \rightarrow {}^4I_{11/2}$ transition, in order to assess its possible use in solid state lasers. For this reason, the absorption and emission cross-sections have also been calculated.

2. Experimental

The fluorotellurite glasses studied in this work presents the following chemical composition (in mol%): $85TeO_2$–$10PbF_2$–$(5-x)AlF_3$–$xNdF_3$ ($x = 0.01$, 0.5 and 2.5), denoted as TeNd001, TeNd05 and TdNd25, respectively. The purities of the substrates are TeO_2 (Aldrich, >99%), PbF_2 (Across Organics, 99.99%), AlF_3 (Aldrich, 99.95%) and NdF_3 (Aldrich, 99.95%). The nominal concentrations of Nd^{3+} ions are 1.51×10^{18}, 7.78×10^{19} and 3.91×10^{20} ions/cm^3, respectively. About 5 g batches of the starting materials were mixed and fully melted in a platinum crucible at 1083 K for 15 min in an electric furnace using air atmosphere. Melts were poured on to a preheated steel plate and then annealed below the T_g temperature (580 K) for 12 h to avoid stress in the material. Prisms with typical dimensions of $10 \times 5 \times 1$ mm^3 were obtained with all their faces carefully polished for the optical characterization, and the density were measured with the Archimedes method using distilled water as the immersion fluid. The refractive indexes have been measured through the apparent thickness method. In order to obtain the wavelength dependence, a polychromatic light with different bandpass filters has been used and the experimental values were fitted following the Cauchy equation:

$$n(\lambda) = A + \frac{B}{\lambda^2} \tag{1}$$

where A and B are coefficients calculated from the curve fitting.

The DSC measurements were carried out on a Perkin Elmer DSC system, heating from room temperature (RT) up to 600 °C at 5 °C/min under nitrogen atmosphere. The analysis of the composition of the obtained glasses has been performed by means of SEM–EDX technique, which confirms the stoichiometric composition of the glasses obtained with differences of less than 10% for the 2.5 mol % of Nd^{3+} glass. Similar results are obtained for the other samples, although the concentration of Nd^{3+} ions was too low to obtain reliable results. The X-ray diffraction patterns were measured in a PANalytical X'Pert PRO diffractometer using the Cu Kα1 (1.5406 Å) radiation in the angular range of $2\theta = 15$–80°, with a step size of 0.02°. The 633 nm Raman data were achieved with a Micro-Raman homemade system equipped with a 632.8 nm Research Electro-Optics Laser He−Ne, 10 mW laser power on sample, a Kaiser OSI MKII Raman head probe coupled to a Nikon Eclipse E600 microscope, and a Nikon 20× objective. An 80 μm spot laser was achieved with this system. The spectra were registered by a Kaiser OSI HoloSpec f/1.8i spectrometer equipped with a diffraction grating for Rayleigh 633 nm and an Andor CCD working at −40 °C. The Raman spectral range spanned from 0 to 3800 cm^{-1}, with best resolution of 5 cm^{-1}. The infrared spectra were obtained with a Perkin Elmer Spectrum 100 FT-IR Spectrometer system equipped with a universal ATR sampling accessory with a spectral resolution of 4 cm^{-1}. The RT absorption spectra of the Nd^{3+}-doped samples were recorded with a spectrophotometer (Perkin Elmer Lambda 9). The luminescence spectra were measured by exciting with cw tunable Ti:sapphire laser (Spectra Physics 3900S) pumped by a CW 532 nm Milennia (Spectra-Physics) laser. The emission was focused onto a 0.32 m monochromator (Jobin Yvon Triax 320) coupled with photomultipliers (Hamamatsu R5108 and H10330B-75). All the luminescence spectra were corrected from instruments response. The luminescence decay curves were obtained by exciting with an optical parametric oscillator OPO (EKSPLA/NT342/3UVE) and recorded and averaged using a digital storage oscilloscope (LeCroy WS424).

3. Theoretical background

The oscillator strengths are proportional to the area under the absorption bands of the RE^{3+} ions, and can be calculated from the experimental absorption spectra in terms of the absorption coefficient $\alpha(\lambda)$ or the optical density (OD) as:

$$f_{exp} = \frac{mc^2}{\pi e^2 N} \int \frac{\alpha(\lambda) d\lambda}{\lambda^2} \tag{2.a}$$

$$\alpha(\lambda) = 2.303 \frac{OD(\lambda)}{d} \tag{2.b}$$

where d is the thickness of the sample; m and e are the mass and charge of the electron, respectively; c is the speed of light; and N is the number of RE^{3+} ions per unit volume (atom/cm^3). According to the J–O theory, the oscillator strength of a transition between an initial (S, L) J manifold and a final (S', L') J' manifold is given by [17,18]:

$$f(aJ;bJ') = \frac{8\pi^2 mc}{3h(2J+1)\lambda e^2 n^2} \{\chi_{ed} S_{ed}(aJ;bJ') + \chi_{md} S_{md}(aJ;bJ')\} \tag{3}$$

$$\chi_{ed} = \frac{n(n^2+2)^2}{9}; \ \chi_{md} = n^3 \tag{4}$$

$$S_{ed}(aJ;bJ') = e^2 \sum_{t=2,4,6} \Omega_t \left\langle f^N[\alpha SL]J \middle\| U^{(t)} \middle\| f^N[\alpha' S'L']J' \right\rangle^2 \tag{5}$$

$$S_{md}(aJ;bJ') = \frac{1}{4}\left(\frac{eh}{2mc}\right)^2 \left\langle f^N[\alpha SL]J \middle\| \vec{L} + 2\vec{S} \middle\| f^N[\alpha' S'L']J' \right\rangle^2 \tag{6}$$

where S_{ed} and S_{md} represent the line strength for the induced electric dipole transitions and the magnetic dipole transitions, respectively [19]. The $\left|\left\langle \left\| U^{(t)} \right\| \right\rangle\right|^2$ parameters are the square of the matrix elements of the unit tensor operators $U^{(t)}$ connecting the initial and final states [17,18]. The intermediate coupling approximation used for the calculation of the matrix elements do not vary significantly between two levels due to the electrostatic shielding of the 4f electrons caused by the closeness of 5p shell electrons. Thus, the matrix elements, reported by Weber et al. and Carnall et al., for the ion can be used for the calculations [19,20]. On the other hand, Neilson and Koster et al. reduced matrix elements for magnetic dipole transitions has been used [21]. The Ω_t ($t = 2, 4, 6$) parameters have a characteristic behavior for a given RE^{3+} ion. Moreover, the three intensity parameters have strong relationship

with the radial wave-functions of the state $4f^N$, the ligand field parameters that characterize the environmental field and the admixing state $4f^{N-1}5d$ and $4f^{N-1}5g$ [22]. The J–O parameters Ω_t were derived from the electric-dipole experimental oscillator strengths using a least-square fitting approach. The magnetic-dipole term only contributes in transition where $\Delta S = \Delta L = 0$ and $\Delta J = \pm 1$ and is independent of the ligand fields. In this work the magnetic-dipolar contributions A_{md} have been calculated using the values given by Weber for the LaF_3 crystal and have been corrected by the refractive index by means of [20]

$$A_{md} = \left(\frac{n}{n'}\right)A'_{md} \tag{7}$$

where primed quantities refer to our glass and the un-primed to the LaF_3 crystal. The spontaneous radiative emission probability A between the J and J' levels for electric- and magnetic-dipole transitions is given by:

$$A(aJ, bJ') = A_{ed} + A_{md} = \frac{64\pi^4}{3h\lambda^3(2J+1)}\left\{\chi_{ed}S_{ed}(aJ; bJ') + \chi_{md}S_{md}(aJ; bJ')\right\} \tag{8}$$

and the radiative lifetime of an excited state and the branching ratios from initial manyfold $|[\alpha SL]J\rangle$ to the lower levels $|[\alpha' S' L']J'\rangle$ are given respectively by

$$\tau_{rad} = \left\{\sum_{bJ'} A(aJ; bJ')\right\}^{-1} \tag{9}$$

$$\beta(aJ, bJ') = \frac{A(aJ, bJ')}{\sum_{bJ'} A(aJ, bJ')} \tag{10}$$

For laser applications, it is convenient to define the emission cross-sections $\sigma_{em}(\lambda)$ that can be determined from the emission spectra by the Fuchtbauer-Landenburg theory through the following formula [23]

$$\sigma_{em}(\lambda) = \frac{\beta_{ij}}{8\pi c n^2 \tau_R} \times \frac{\lambda^5 I(\lambda)}{\int \lambda I(\lambda) d\lambda} \tag{11}$$

Once the $\sigma_{em}(\lambda)$ is known, the absorption cross-section $\sigma_{abs}(\lambda)$ of the gain media it can be obtained through the McCumber theory [23,24]

$$\sigma_{em}(\lambda) = \sigma_{abs}(\lambda)\exp\left[\frac{(\varepsilon - h\nu)}{KT}\right] \tag{12}$$

where h is the Planck constant; K the Boltzmann constant; and ε the net free energy required to excite one Nd^{3+} in the following transitions $^4F_{3/2} \rightarrow {}^4I_{13/2}$, $^4F_{3/2} \rightarrow {}^4I_{11/2}$, $^4F_{3/2} \rightarrow {}^4I_{9/2}$ at temperature T. Furthermore, it is also interesting to define the effective emission cross-section $\sigma_{eff}(\lambda_0)$ as [25]:

$$\sigma_{eff}(\lambda_0) = \frac{\lambda_0^4}{8\pi c n^2 \Delta\lambda_{eff}} A(aJ; bJ') \tag{13}$$

where λ_0 is the emission peak and $\Delta\lambda_{eff}$ the emission linewidth define as

$$\Delta\lambda_{eff} = \frac{\int \sigma_{eff}(\lambda) d\lambda}{\sigma_e^{peak}} \tag{14}$$

Moreover, it is possible to define the optical gain cross section $G(\lambda)$ from the absorption and emission cross-sections. The definition can be done by a simplified two energy levels model, for which one can assume that the whole population of the Nd^{3+} ions is delivered between the ground state level 1 and the excited state level 2. In this regard, the optical gain can be related with the absorption and emission cross-sections through the population inversion parameter (γ), defined as the number of Nd^{3+} ions excited state respect to the total number of Nd^{3+} ions, which is expressed as [26]:

$$G(\lambda) = \gamma\sigma_{em}(\lambda) - (1-\gamma)\sigma_{abs}(\lambda) \tag{15}$$

4. Results and discussions

4.1. X-ray diffraction and DSC measurements

The X-ray powder diffraction pattern of the glass reveals no sharp crystallization peaks and three broad bands with peaks at 6.5°, 28° and 50° 2θ, independent of the Nd^{3+} concentration, which confirms the amorphous nature of the prepared glass (see Fig. 1). Such broad peaks are due to the dopant element, i.e. neodymium. DSC measurements show a curve with two endothermic peaks corresponding to a glass transition at about 400 °C and to the melting point of the tellurite at about 560 °C (see Fig. 1).

4.2. Raman spectra

It is known that the radiative properties of the RE^{3+} depend on the phonon energy of the host in which are embedded, in such a way that the lower the energy phonon, the larger the radiative probabilities of transitions. Raman spectra allow us to obtain the spectrum corresponding to the energy phonons of the host. Results indicate that we are dealing with a relatively low energy phonon host, with a maximum value less than 750 cm^{-1}, appropriate for laser applications. As can be observed in Fig. 2, the Raman spectra of the Nd^{3+}-doped fluotellurite consist in four overlapped bands. At first glance, one can observe the symmetric Te–O–Te intra-chain bridges, where such bridges are typical on complex tellurite anions [5,27] and the possible vibrations of the heavy metal fluoride. The bands under 300 cm^{-1} correspond to the optical modes of TeO_2 such as the translatory and rotatory (or librations) vibrations, however the collective modes of the local structures and heavy metal vibrational modes of the (PbF_2) and (AlF_3) could be also attributed [28–30]. The bands from 250 cm^{-1} to 700 cm^{-1} can be assigned to the vibrational modes of the stretching vibrations of TeO_{3+1} and TeO_4, where the most intense band at ~450 cm^{-1} corresponds to the symmetric stretching vibrations of Te–O–Te intra-chain bridges and the band at 660 cm^{-1} is generated by the stretching vibrations of TeO_4. On the other hand, the asymmetric stretching at 750 cm^{-1} can be assigned to the TeO_3 and/or TeO_{3+1} trigonal pyramids [31,32]. The oxyfluoride glasses present the

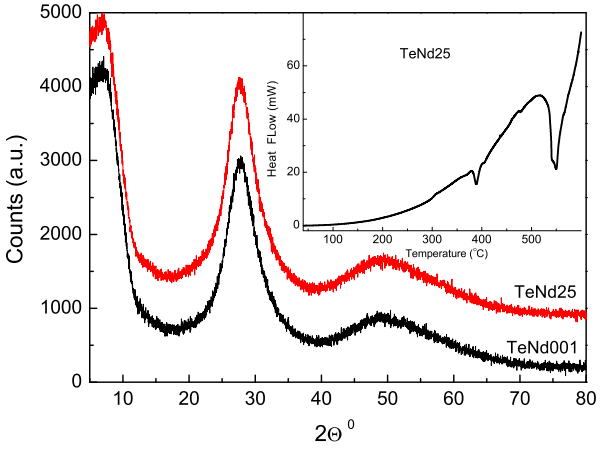

Fig. 1. XRD pattern of glass Nd^{3+}-doped fluorotellurite and DSC measurement (inset).

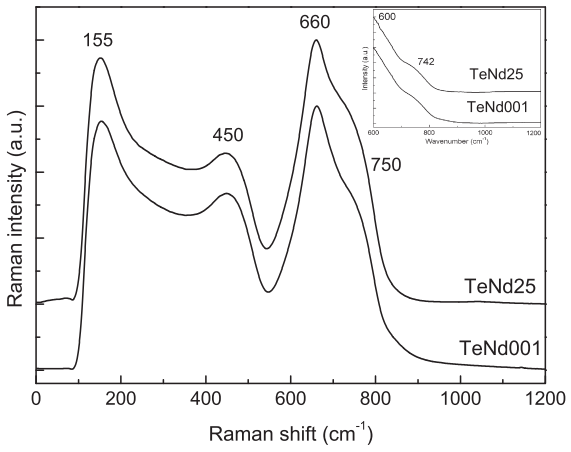

Fig. 2. Raman spectra at 633 nm laser wavelength and IR spectra (inset) of the Nd^{3+} ions in TeO_2–PbF_2–AlF_3 glasses.

IR-vibrational behavior corresponding to the TeO_2 composition material, where the bands at 600 cm^{-1} and 742 cm^{-1} are attributed to the stretching mode [TeO_4] trigonal pyramidal with bridging oxygen and the stretching mode of [TeO_3] trigonal pyramidal with non-bridging oxygen, respectively [33].

4.3. Optical absorption and luminescence

The RT absorption spectrum of the TeNd25 fluorotellurite has been obtained from 350 to 1000 nm and it is presented in Fig. 3. For the other samples, TeNd001 and TeNd05, the only difference observed, with respect to that presented, is the optical density of the bands, which is proportional to the concentration of Nd^{3+} ions. The spectra show the main bands corresponding to the $4f^3$–$4f^3$ intra-configurational electronic transitions from the ground state $^4I_{9/2}$ to the excited states, which have been ascribed as follows in order of increasing energy: $^4F_{3/2}$, ($^4F_{5/2}$, $^2H_{9/2}$),($^4F_{7/2}$, $^4S_{3/2}$), $^4F_{9/2}$, $^2H_{11/2}$, ($^4G_{5/2}$, $^2G_{7/2}$), $^4G_{7/2}$, $^2G_{9/2}$, ($^4G_{9/2}$, $^2D_{3/2}$, $^4G_{11/2}$) and $^2P_{1/2}$. Due to the overlapping of some of the absorption bands, the assignment cannot be accurately made. Up to nine bands were used to fit the J–O parameters Ω_t. Slight differences were observed changing the Nd^{3+} concentration, therefore, the results obtained for the TeNd25 glass were used ever since. In Table 1 the theoretical oscillator strengths obtained fitting to Eq. (6) are shown and compared to the experimental ones, with a reasonable good agreement between them as can be observed from the RMS deviation. According to other authors, the $^4I_{9/2} \rightarrow {}^4G_{5/2}$, $^2G_{7/2}$ hypersensitive transition at 585 nm (17,100 cm^{-1}) is the most intense one, as can be observed in other tellurites, fluorophosphates and bismuth borated glasses [5,6,13,34], and are governed by the quadrupole selection rules ($|\Delta S| \leqslant 0, |\Delta L|, |\Delta J| \leqslant 2$) [35,21].

Table 1
Barycenter of the absorption bands and the Judd Ofelt parameters of the Nd^{3+} ions in TeO_2–PbF_2–AlF_3 glasses. Experimental and calculated oscillators strength are also shown.

$^4I_{9/2}\rightarrow$	Barycenter (cm^{-1})	$f_{exp} \times 10^{-8}$	$f_{cal} \times 10^{-8}$ (n = cte)	$f_{cal} \times 10^{-8}$ ($n \neq$ cte)
$^4F_{3/2}$	11,494	300	467	441
$^4F_{5/2}$, $^2H_{9/2}$	12,437	1316	1314	1276
$^4F_{7/2}$, $^4S_{3/2}$	13,404	1240	1266	1290
$^4F_{9/2}$	14,641	97	100	101
$^2H_{11/2}$	15,938	24	28	29
$^2G_{7/2}$, $^4G_{5/2}$	17,094	3327	3338	3336
$^4G_{7/2}$ $^2G_{9/2}$	19,455	1200	1052	1092
$^4G_{9/2}$, $^2D_{3/2}$, $^4G_{11/2}$	21,097	256	257	277
$^2P_{1/2}$	23,201	92	124	134
Refractive index n			2.14	1.928 + 44,589/λ^2
Ω_2			4.21×10^{-20}	4.51×10^{-20}
Ω_4			5.97×10^{-20}	6.34×10^{-20}
Ω_6			5.45×10^{-20}	6.16×10^{-20}
Rms			9.26×10^{-7}	7.74×10^{-7}
Density			3.9130×10^{20} ions/cm^3	

The emission spectra of the Nd^{3+}-doped fluorotellurite glasses as a function of Nd^{3+} concentration have been obtained under a cw 805 nm laser excitation, in resonance with the $^4I_{9/2} \rightarrow$ ($^4F_{5/2}$, $^2H_{9/2}$) transitions, that immediately populates the $^4F_{3/2}$ state via multiphonon de-excitation of the Nd^{3+} ions (see Fig. 4). The low concentrated glass shows three different bands with barycenters around 950 nm, 1065 nm and 1340 nm, ascribed to the $^4F_{3/2} \rightarrow {}^4I_{9/2}$, $^4I_{11/2}$, $^4I_{13/2}$ transitions, respectively. For comparison with the other Nd^{3+} concentrated glasses, the spectra have been normalized to the more intense band $^4F_{3/2} \rightarrow {}^4I_{11/2}$. The lack of structure in the bands and their widths are again a clear evidence of the multiple different environments felt by the Nd^{3+} ions which is typical in glassy systems. When the Nd^{3+} ions concentration increases another band appears at 1180 nm, which can be

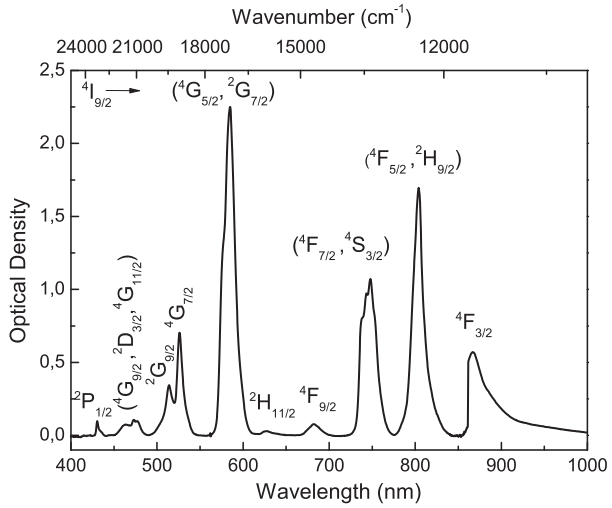

Fig. 3. Absorption spectrum of TeNd25 glass at RT.

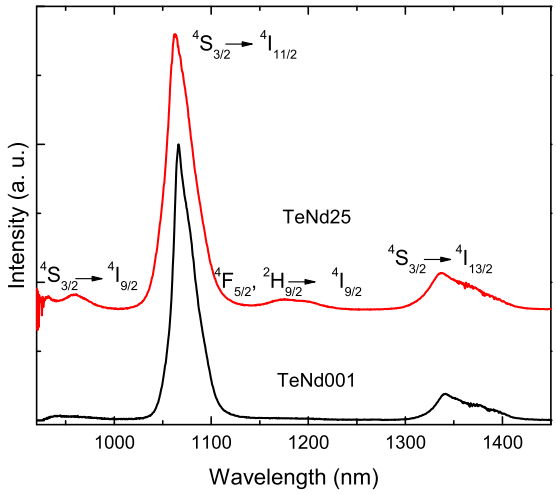

Fig. 4. RT emission spectra of the TeNd001 and TeNd25.

associated with the ($^4F_{5/2}$, $^2H_{9/2}$) → $^4I_{13/2}$ transition, and there is also a broadening of the band associated with the $^4F_{3/2}$ → $^4I_{11/2}$.

4.4. Decay of the luminescence

The decay curves of the $^4F_{3/2}$ → $^4I_{11/2}$ transition have been obtained for the three different concentrations, pumping at 800 nm (Fig. 5). For the TeNd001 and TeNd05 glasses, the curves show a quasi-exponential behavior that can be associated with the distribution of environments for the Nd^{3+} ions in the glassy systems, although the decay curve for the TeNd25 is highly non-exponential. For this reason, the experimental decay time was calculated as an average lifetime defined as

$$\tau_{exp} = \frac{\int_0^\infty t \cdot I(t)dt}{\int_0^\infty I(t)dt} \quad (16)$$

where $I(t)$ is the intensity of the decay curve. The calculated lifetimes obtained were 174, 122 and 85 μs for the TeNd001, TeNd05 and TeNd25, respectively (see inset of Fig. 5). On the other hand, the radiative lifetime τ_{rad} (Eq. (9)) for the $^4F_{3/2}$ state was obtained from the J–O fittings, resulting in 257.6 μs (see Table 2). With these experimental data a rough estimation of the different contributions of the non-radiative mechanisms taking part in the de-excitation processes can be calculated through the following equation,

$$\frac{1}{\tau_{exp}} = \frac{1}{\tau_{rad}} + W_{NR} = \frac{1}{\tau_{rad}} + W_{MP} + W_{ET} \quad (17)$$

where non-radiative probability W_{NR} has been separated into its major contributions, i.e. the multiphonon relaxation probability W_{MP}, which is dependent on the host but not on the concentration of dopant [36,37], and the energy transfer probability W_{ET}, which depends on the dopant ion concentration. For the TeNd001 glass, W_{ET} term can be neglected since this term decreases with the sixth power of the distances between Nd^{3+} ions, therefore for such a low dopant concentration (0.001 mol%), large distances between them are expected. Consequently, and taking into account Eq. (17), W_{MP} can be estimated from the lifetimes τ_{exp} and τ_{rad}, this gives approximately 1865 s^{-1}, which not depend on concentration. For the other glasses, TeNd05 and TeNd25, the drop of the lifetimes, which is more than double for TeNd25 respect to TeNd001, and the highly non-exponential curve (see Fig. 5), are related to the enhancement of W_{ET} with Nd^{3+} concentration, induced by the shortening of the Nd^{3+}–Nd^{3+} distances due to the increase in the concentration of Nd^{3+} ions present in the glass. Therefore, once W_{MP} has been fixed,

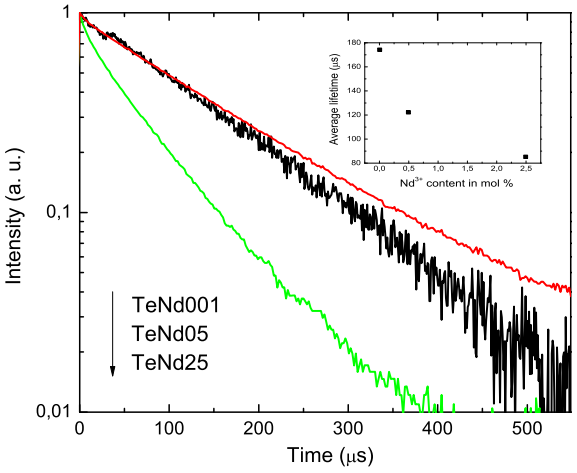

Fig. 5. Decay curves of the $^4F_{3/2}$ → $^4I_{11/2}$ transition as a function of Nd^{3+} concentration at RT. The inset shows the calculated average lifetimes.

Table 2
Spontaneous radiative transition rates, branching ratios and radiative lifetimes of the Nd^{3+} ions in TeO_2–PbF_2–AlF_3 glasses.

Transitions	A (s^{-1})	β (%)	τ_{rad} (μs)
$^4F_{7/2}$ → $^4F_{5/2}$	0.27	0.00001	90.6
$^4F_{3/2}$	3.25	0.0003	
$^4I_{15/2}$	1199.10	0.1087	
$^4I_{13/2}$	1258.97	0.1141	
$^4I_{11/2}$	3526.72	0.3196	
$^4I_{9/2}$	5047.93	0.4574	
$^4F_{5/2}$ → $^4F_{3/2}$	0.66	0.0001	90.2
$^4I_{15/2}$	342.98	0.0309	
$^4I_{13/2}$	2047.18	0.1847	
$^4I_{11/2}$	1418.16	0.1279	
$^4I_{9/2}$	7276.23	0.6564	
$^4F_{3/2}$ → $^4I_{15/2}$	18.38	0.0047	257.6
$^4I_{13/2}$	364.9	0.0940	
$^4I_{11/2}$	1633.25	0.4208	
$^4I_{9/2}$	1864.75	0.4804	

W_{ET} was calculated with values of 2383 s^{-1} and 6018 s^{-1}, respectively.

Other important parameter for laser applications is the quantum efficiency of emission (η), that can be estimated from the lifetimes measurements through the following expression

$$\eta = \frac{W_{rad}}{W_{rad} + W_{NR}} = \frac{\tau_{exp}}{\tau_{rad}} \quad (18)$$

In our case, η values obtained for the $^4F_{3/2}$ → $^4I_{11/2}$ transition in the Nd^{3+} doped glasses are 0.67, 0.48 and 0.33 for the TeNd001, TeNd05 and TeNd25, respectively.

4.5. Laser properties

In order to test the possible application of these glasses as laser gain media some parameters were calculated. On one hand, the spectroscopic quality factor $\chi = \Omega_4/\Omega_6$ defined by Kaminskii [38]. In our case, the transitions from the metastable $^4F_{3/2}$ state depend only on the Ω_4 and Ω_6 parameters, due to the zero value of the matrix elements of the operator $\langle \| U^{(t)} \| \rangle$ of rank 2 between the $^4F_{3/2}$ and ^4I_J (J = 9/2, 11/2, 13/2 and 15/2) states, this factor is used to check the availability of the matrix as candidates for laser applications, since characterizes the possibility of attaining stimulated emission from a particular transition. In the case of the most intense emission band for the Nd^{3+}, corresponding to the $^4F_{3/2}$ → $^4I_{9/2}$ transition, low values of χ are required (see Table 3). In our case, a relative low value of χ (1.07) has been found, compared to other glasses proposed as laser gain media (see Table 3). On the other hand, the stimulated emission cross-section $\sigma_{em}(\lambda)$ has also been calculated from the emission spectra, through the Fuchtbauer-Ladenburg equation (Eq. (11)). The values obtained for the three Nd^{3+} concentrations, which in the maxima coincide with those of $\sigma_{eff}(\lambda_0)$ (Eq. (13)), are presented in Table 3, and are

Table 3
Experimental parameters obtained for the $^4F_{3/2}$ → $^4I_{11/2}$ transition of Nd^{3+}. The χ, $\sigma_{eff}(\lambda_0)$ and $\Delta\lambda_{eff}$ are compared with other glasses.

Glass	χ	$\sigma_{eff}(\lambda_0)$ ($\times 10^{-20}$ cm^2)	$\Delta\lambda_{eff}$ (nm)	Refs.
TeNd25	1.07	1.67	37.6	This work
TeNd05		2.05	30.5	
TeNd001		2.08	29.9	
NKZLSNd10	1.05	4.30	38	[34]
TZNLN	0.86	4.27	28	[39]
Fluoroborates	1.13	4.94	22	[6]
Oxyfluorides CaF_2	1.36	2.27	33	[40]

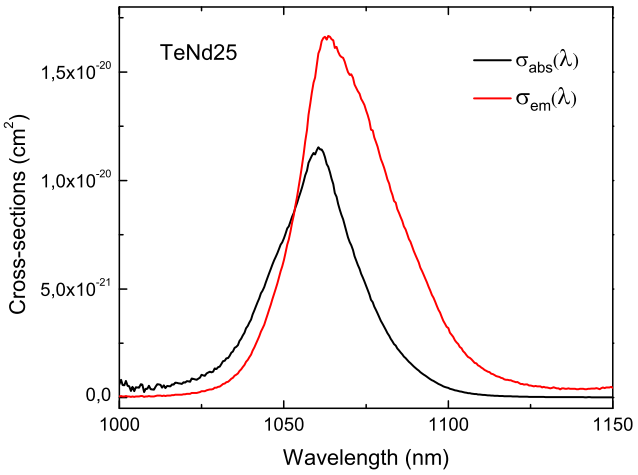

Fig. 6. Absorption and spontaneous emission cross-sections of the $^4F_{3/2} \rightarrow {}^4I_{11/2}$ transition for the TeNd25 glass.

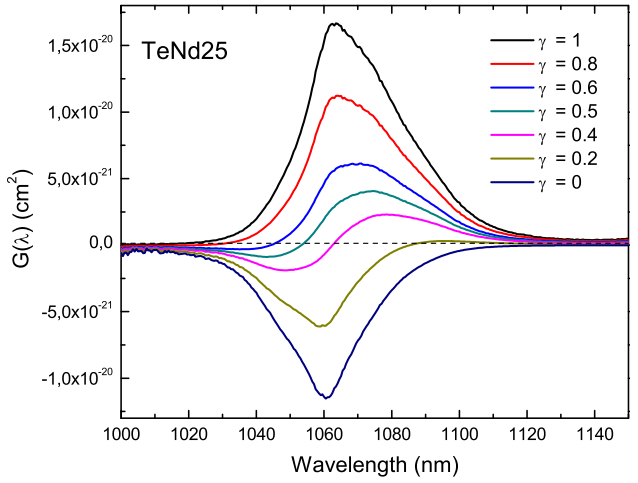

Fig. 7. Gain coefficient cross-section $G(\lambda)$ of the $^4F_{3/2} \rightarrow {}^4I_{11/2}$ transition as a function of the population inversion parameter for the TeNd25 glass.

similar to other glass compositions. Once the $\sigma_{em}(\lambda)$ was calculated, the absorption cross section $\sigma_{abs}(\lambda)$ can be obtained using the McCumber theory (Eq. (12)); the results for the TeNd25 are depicted in Fig. 6. Moreover and taking advantage of the previous cross section parameters calculated, the optical gain cross-section $G(\lambda)$ was obtained using Eq. (15) and is depicted in Fig. 7 for the TeNd25 glass; similar results have been obtained for the other glasses. It starts having a nearly flat and positive value for a population inversion factor γ of 0.4 in the spectral range from 1060 to 1110 nm.

5. Conclusions

A complete study of the characterization of Nd^{3+}-doped TeO_2–PbF_2–AlF_3 glasses for different concentration of dopant has been carried out. Especial attention has been paid to the optical properties. The absorption and emission spectra as well as the X-ray diffraction measurements indicate a glassy environment for the Nd^{3+} ions. From the J–O theory the radiative lifetime τ_{rad} of the $^4F_{3/2}$ state was obtained and compared with the experimental one τ_{exp}; this allows us to estimate the W_{MP} (1865 s^{-1}) and the W_{ET} as a function of the Nd^{3+} concentration, 2383 s^{-1} and 6018 s^{-1}, for TeNd05 and TeNd25, respectively. Exploring the possibility of using this Nd^{3+}-doped glass for laser applications, different parameters were calculated, quantum efficiencies of emission η for the $^4F_{3/2} \rightarrow {}^4I_{13/2}$ transition ranging from 0.68 to 0.33 as a function of concentration were found. On the other hand a relative low value of the spectroscopic quality factor χ (1.07) was obtained. Furthermore, the $\sigma_{em}(\lambda)$ profiles, as well as the $\sigma_{eff}(\lambda_0)$ were obtained from emission spectra with values of 2.08×10^{-20} cm^2, 2.05×10^{-20} cm^2 and 1.66×10^{-20} cm^2 for the TeNd001, TeNd05 and TeNd25, respectively, this values are relatively high compared with other glasses proposed as laser hosts. Finally the gain emission cross section $G(\lambda)$ was also calculated for the three glasses and a population inversion factor of 0.4 was found for the $^4F_{3/2} \rightarrow {}^4I_{13/2}$ transition.

Acknowledgements

This work has been partially supported by MINECO under The National Program of Materials (MAT2013-46649-C4-4-P), the Consolider-Ingenio 2010 Program (MALTA CSD2007-00045) and by Fundación CajaCanarias (ENER-01).

References

[1] J. Lucas, P. Lucas, T. Le Mercier, A. Rollat, W. Davenport, Rare Earths, Elsevier, 2015. doi:10.1016/B978-0-444-62735-3.00016-4.
[2] G. Brambilla, H.H. Kee, V. Pruneri, T.P. Newson, Optical fibre sensors for earth sciences, Opt. Lasers Eng. 37 (2002) 215–232, http://dx.doi.org/10.1016/S0143-8166(01)00096-3.
[3] C. Madhukar Reddy, B. Deva Prasad Raju, N. John Sushma, N.S. Dhoble, S.J. Dhoble, Renew. Sustain. Energy Rev. 51 (2015) 566–584, http://dx.doi.org/10.1016/j.rser.2015.06.025.
[4] F. Lahoz, I.R. Martín, U.R. Rodríguez-Mendoza, I. Iparraguirre, J. Azkargorta, A. Mendioroz, et al., Rare earths in nanocrystalline glass–ceramics, Opt. Mater. 27 (2005) 1762–1770, http://dx.doi.org/10.1016/j.optmat.2004.11.047.
[5] A. Jha, B. Richards, G. Jose, T. Teddy-Fernandez, P. Joshi, X. Jiang, et al., Prog. Mater Sci. 57 (2012) 1426–1491, http://dx.doi.org/10.1016/j.pmatsci.2012.04.003.
[6] R.T. Karunakaran, K. Marimuthu, S. Arumugam, S. Surendra Babu, S.F. Leon-Luis, C.K. Jayasankar, Opt. Mater. 32 (2010) 1035–1041, http://dx.doi.org/10.1016/j.optmat.2010.02.026.
[7] U.R. Rodríguez-Mendoza, E.A. Lalla, J.M. Cáceres, F. Rivera-López, S.F. León-Luís, V. Lavín, J. Lumin. 131 (2011) 1239–1248, http://dx.doi.org/10.1016/j.jlumin.2011.02.020.
[8] M.V.D. Vermelho, P.V. dos Santos, M.T. de Araújo, A.S. Gouveia-Neto, F.C. Cassanjes, S.J.L. Ribeiro, et al., J. Lumin. 102-103 (2003) 762–767, http://dx.doi.org/10.1016/S0022-2313(02)00638-5.
[9] C. Strümpel, M. McCann, G. Beaucarne, V. Arkhipov, A. Slaoui, V. Švrček, et al., Sol. Energy Mater. Sol. Cells 91 (2007) 238–249, http://dx.doi.org/10.1016/j.solmat.2006.09.003.
[10] W. Wang, X. Lei, H. Gao, Y. Mao, Opt. Mater. (Amst). 47 (2015) 270–275, http://dx.doi.org/10.1016/j.optmat.2015.05.040.
[11] J. Nelson, The Physics of Solar Cells, Wolrd Scientific, Imperial College Press, 2003.
[12] F. Yang, C. Liu, D. Wei, Y. Chen, J. Lu, S. Yang, Opt. Mater. (Amst). 36 (2014) 1040–1043, http://dx.doi.org/10.1016/j.optmat.2014.01.020.
[13] J. Pisarska, W.A. Pisarski, W. Ryba-Romanowski, Opt. Laser Technol. 42 (2010) 805–809, http://dx.doi.org/10.1016/j.optlastec.2009.12.008.
[14] Y. Qiao, N. Da, D. Chen, Q. Zhou, J. Qiu, T. Akai, Appl. Phys. B 87 (2007) 717–722, http://dx.doi.org/10.1007/s00340-007-2637-3.
[15] L. Jyothi, V. Venkatramu, P. Babu, C.K. Jayasankar, M. Bettinelli, G. Mariotto, A. Speghini, Opt. Mater. (Amst). 33 (2011) 928–936, http://dx.doi.org/10.1016/j.optmat.2010.11.015.
[16] J.S. Sanghera, L. Brandon Shaw, I.D. Aggarwal, IEEE J. Sel. Top. Quant. Electron. 15 (2009) 114–119, http://dx.doi.org/10.1109/JSTQE.2008.2010245.
[17] G.S. Ofelt, J. Chem. Phys. 37 (1962) 511–520.
[18] B.R. Judd, Phys. Rev. 127 (1962) 750–761, http://dx.doi.org/10.1103/PhysRev.127.750.
[19] W.T. Carnall, P.R. Fields, K. Rajnak, J. Chem. Phys. 49 (1968) 4412.
[20] M.J. Weber, Phys. Rev. 157 (1967) 262–272, http://dx.doi.org/10.1103/PhysRev.157.262.
[21] R. Van Deun, K. Binnemans, C. Görller-Walrand, J.L. Adam, J. Alloys Compd. 283 (1999) 59–65, http://dx.doi.org/10.1016/S0925-8388(98)00895-0.
[22] M.P. Hehlen, M.G. Brik, K.W. Krämer, J. Lumin. 136 (2013) 221–239, http://dx.doi.org/10.1016/j.jlumin.2012.10.035.
[23] D.E. McCumber, Phys. Rev. 136 (1964) A954–A957, http://dx.doi.org/10.1103/PhysRev.136.A954.
[24] W.J. Miniscalco, R.S. Quimby, Opt. Lett. 16 (1991) 258–260, http://dx.doi.org/10.1364/OL.16.000258.
[25] M.J. Weber, D.C. Ziegler, C.A. Angell, J. Appl. Phys. 53 (1982) 4344.

[26] J.F. Philipps, T. Töpfer, H. Ebendorff-Heidepriem, D. Ehrt, R. Sauerbrey, N.F. Borrelli, Appl. Phys. B 72 (2001) 175–178, http://dx.doi.org/10.1007/s003400000415.
[27] G.S. Murugan, T. Suzuki, Y. Ohishi, J. Appl. Phys. 100 (2006) 023107, http://dx.doi.org/10.1063/1.2215218.
[28] U. Gross, S. Rüdiger, E. Kemnitz, K.-W. Brzezinka, S. Mukhopadhyay, C. Bailey, A. Wander, N. Harrison, J. Phys. Chem. A 111 (2007) 5813–5819, http://dx.doi.org/10.1021/jp072388r.
[29] V. Rodriguez, M. Couzi, F. Adamietz, M. Dussauze, G. Guery, T. Cardinal, P. Veber, K. Richardson, P. Thomas, J. Raman Spectrosc. 44 (2013) 739–745, http://dx.doi.org/10.1002/jrs.4251.
[30] P. Thangadurai, S. Ramasamy, R. Kesavamoorthy, J. Phys.: Condens. Matter 17 (2005) 863–874, http://dx.doi.org/10.1088/0953-8984/17/6/007.
[31] C.J. Hill, A. Jha, J. Non-Cryst. Solids 353 (2007) 1372–1376, http://dx.doi.org/10.1016/j.jnoncrysol.2006.10.061.
[32] A. Jha, S. Shen, M. Naftaly, Phys. Rev. B 62 (2000) 6215–6227, http://dx.doi.org/10.1103/PhysRevB.62.6215.
[33] S. Rada, A. Dehelean, E. Culea, J. Non-Cryst. Solids 357 (2011) 3070–3073, http://dx.doi.org/10.1016/j.jnoncrysol.2011.04.013.
[34] D. Ramachari, L. Rama Moorthy, C.K. Jayasankar, Infrared Phys. Technol. 67 (2014) 555–559, http://dx.doi.org/10.1016/j.infrared.2014.09.020.
[35] B. Klimesz, G. Dominiak-Dzik, M. Żelechower, W. Ryba-Romanowski, Opt. Mater. (Amst). 30 (2008) 1587–1594, http://dx.doi.org/10.1016/j.optmat.2007.09.011.
[36] G. Blasse, B.C. Grabmaier, Luminescent Materials, 1st ed., Springer-Verlag Berlin Heidelberg, Berlin, 1994.
[37] C.B. Layne, W.H. Lowdermilk, M.J. Weber, Phys. Rev. B 16 (1977) 10–20, http://dx.doi.org/10.1103/PhysRevB.16.10.
[38] A.A. Kaminskii, L. Li, Pisma v Zhurnal Tekhnischeskoi Fiz. – Sov. Tech. Phys. Lett. 1 (1975) 567–571. 256–258.
[39] S. Surendra Babu, R. Rajeswari, K. Jang, C. Eun Jin, K. Hyuk Jang, H. Jin Seo, J. Jayasankar, J. Lumin. 130 (2010) 1021–1025, http://dx.doi.org/10.1016/j.jlumin.2010.01.017.
[40] D. Chen, Y. Wang, Y. Yu, E. Ma, F. Liu, J. Phys. Chem. Solids 68 (2007) 193–200, http://dx.doi.org/10.1016/j.jpcs.2006.10.009.